Lawrence Berkeley Laboratory
UNIVERSITY OF CALIFORNIA

Materials & Molecular
Research Division

Submitted to the Journal of Chemical Physics

A CRITICAL TEST OF VIBRATIONAL DEPHASING THEORIES IN SOLIDS USING SPONTANEOUS RAMAN SCATTERING IN ISOTOPICALLY MIXED CRYSTALS

S. Marks, P. A. Cornelius and C. B. Harris

April 1980

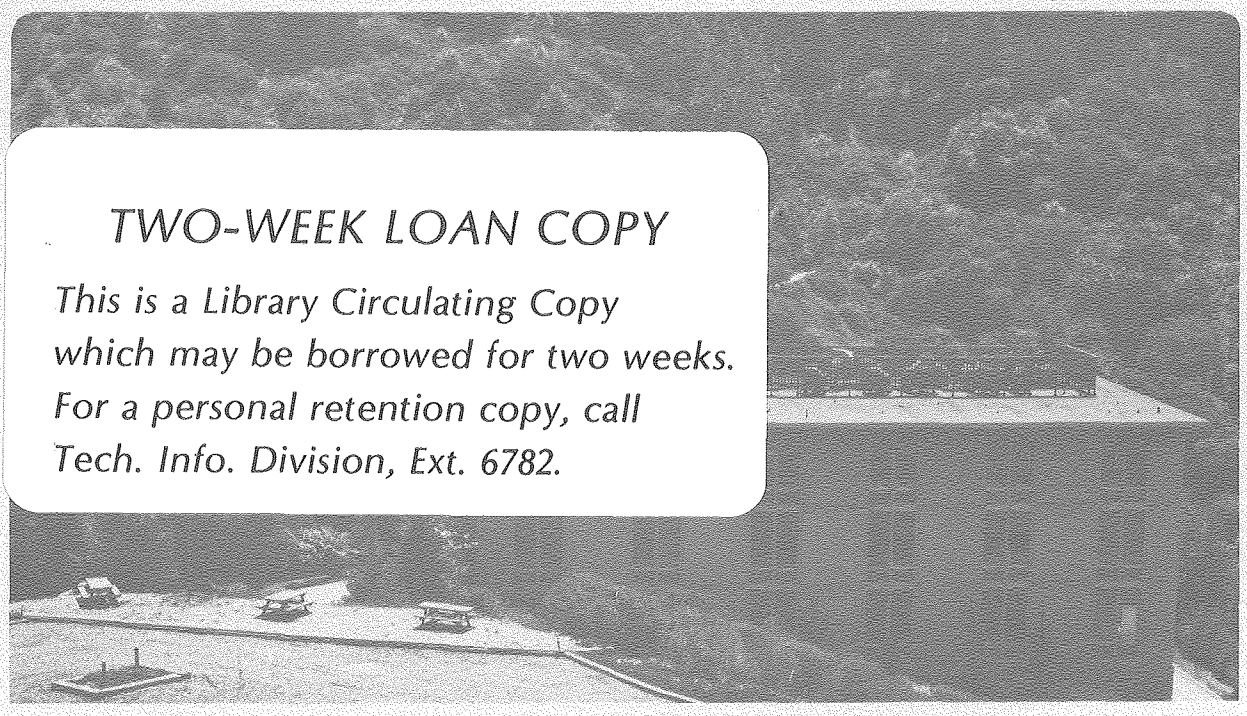

Prepared for the U.S. Department of Energy under Contract W-7405-ENG-48

DISCLAIMER

LBL #10181
Submitted to Journal of Chemical Physics

A CRITICAL TEST OF VIBRATIONAL DEPHASING THEORIES IN SOLIDS USING SPONTANEOUS RAMAN SCATTERING IN ISOTOPICALLY MIXED CRYSTALS

S. Marks, P. A. Cornelius and C. B. Harris

Department of Chemistry
University of California

and

Molecular Materials Research Division
Lawrence Berkeley Laboratory
Berkeley, California 94720

ABSTRACT

A series of experiments has been conducted in order to evaluate the relative importance of several recent theories of vibrational dephasing in solids. The theories are discussed briefly, and are used to interpret the temperature dependence of the C-H and C-D stretch bands in the spontaneous Raman spectra of h_{14}- and d_{14}-1,2,4,5-tetramethyl benzene (durene). The infrared spectra of these same molecules are also reported in the region of the combination bands involving C-H (or C-D) stretches and low-frequency modes. The results support the applicability of the model of Harris, et. al.[1-3], based on energy exchange in anharmonically coupled low-frequency modes. This theory is then used, in connection with Raman spectra obtained in isotopically mixed samples of durene, to elucidate the vibrational dynamics underlying the dephasing. It is found that the results are consistent with the hypothesis that some low-frequency modes in this molecule are significantly delocalized or "excitonic" in character, and that this delocalization may be studied by means of Raman spectroscopy on the low-frequency modes themselves, as well as by exchange analysis of the coupled high-frequency modes. These conclusions represent a generalization and extension of the previously published[3] exchange model.

I. Introduction

Processes which cause dephasing of spectroscopic transitions have been under investigation for many years. Analysis of lineshapes has, in many instances, provided an understanding of molecular correlations, dynamics, and structure. A large body of theoretical work[1-31] exists to assist in the interpretation of experimental spectra, and to illuminate the fundamental interactions responsible for dephasing.

The specific question of vibrational dephasing in solids, to which a great deal of recent activity has been directed,[1-3,29-31] is complicated by two general facts: 1) the dephasing time (T_2) of a vibrationally excited molecule in a condensed phase is very short (typically 1-10 picoseconds);[4] and 2) intermolecular forces are always present in the condensed phase, making difficult the interpretation of experimental results and the development of theoretical models. Because of this, experimental work bearing on this problem has consisted primarily of spontaneous Raman lineshape studies, and some picosecond laser measurements in liquids[4,32] and in solid calcite;[33] while theoretical treatments of vibrational dephasing have, in general, relied upon a stochastic description of the relevant many-body dynamics.

An understanding of vibrational dephasing in solids requires both the construction of theoretical models and the experimental determination of which mechanisms and interactions are important. In a previous series of papers,[1-3] we have presented data obtained from the temperature-dependent spontaneous Raman spectrum of h_{14}-1,2,4,5 tetramethylbenzene (durene), and successfully interpreted this data by developing a theory based on intermolecular energy exchange by low-frequency vibrational modes (hereafter referred to as HSC exchange). Recent theoretical work[29-31] has made it

possible to design a further series of experiments in order to test more conclusively the HSC exchange hypothesis, and to compare that model with two other theories: one by Abbott and Oxtoby[31] based on interactions between pairs of vibrational fundamentals (AO), and the other by Wertheimer[30] based on the mechanism of dynamic coupling (DC).

The purpose of this paper is three-fold. First of all, we review the three theories mentioned above, with an emphasis on how they may be distinguished experimentally. Second, we present experimental results of three types: the temperature dependence of the Raman spectrum of pure d_{14}-durene, which complements our previously published work on h_{14}-durene; the concentration dependence of the d_{14}-durene spectrum as it is successively diluted in h_{14}-durene; and the infrared spectrum of both molecules in the region where HSC exchange predicts the presence of combination levels. These results are discussed in terms of the three theoretical models. Third, we use the parameters obtained from HSC exchange analysis, combined with other spectral evidence, to support a delocalized or "exciton" model for the dynamics of the low-frequency modes.

This paper is organized as follows: In Section II we review the three theories mentioned above and compare their experimental predictions. Section III describes our experimental procedures. Section IV presents experimental results, along with a discussion of the relative importance of the dephasing mechanisms treated by the theoretical models of Section II. Section V presents further results and an analysis of the energy transfer dynamics of the durene system we have studied, including the evidence in support of a vibrational exciton model. Section VI summarizes the most important general conclusions of the work.

II. Theoretical Treatments of Vibrational Dephasing in Condensed Phase

A. Interaction of a Fundamental and Its Hot Band - HSC Exchange

Figure 1 shows a high-frequency mode A and a low-frequency mode B. Because of anharmonic coupling between the two modes, the energy of the combination level ($n_A = 1$, $n_B = 1$) does not equal the sum of the energies of the singly excited levels ($n_A = 1$, $n_B = 0$ and $n_A = 0$, $n_B = 1$). Thus the transition frequency of mode A depends on the state of mode B; restricting the discussion to the four level system in the diagram implies that there are two possible transition frequencies for mode A: ω_o when B is unexcited, and $\omega_o + \delta\omega$ when B is excited. The presence of energy exchange, indicated by the arrows in the diagram, will modulate the frequency of the high frequency mode A, as mode B becomes excited and deexcited. This energy exchange process of mode B is incorporated into the temperature-dependent broadening and frequency shift of the Raman or infrared transition associated with mode A.

Using a reduced density matrix approach and the assumption of Markovian statistics (detailed elsewhere),[3] the lineshape function may be obtained. In the low-temperature limit this reduces to the following approximate expressions for the lineshape $I(\omega)$:

$$I(\omega) = \frac{I(\omega^{eff})}{1 + (\omega-\omega^{eff})^2(T_2^{eff})^2} \qquad (1)$$

where the effective Raman frequency is

$$\omega^{eff} = \omega_o + \frac{e^{-E_i/kT}\delta\omega}{(1 + (\delta\omega)^2\tau^2)} \qquad (2)$$

and the effective linewidth is

$$(T_2^{eff})^{-1} = (T_2)^{-1} + \frac{e^{-E_i/kT}(\delta\omega)^2\tau}{(1 + (\delta\omega)^2\tau^2)} \qquad (3)$$

The important points to note are: 1) Both the width and shift display the same apparent "activation energy", E_i, which is equal to the energy of a quantum of mode B. 2) The quantities $\delta\omega$,τ and E_i can be extracted from a temperature dependent study of the linewidth and peak frequency of the mode A spectrum. The physical meaning of τ, which in this simple discussion is the lifetime of the low frequency mode B, will be examined below in greater detail. 3) Detailed balance requires that the intermolecular exchange rate of a quantum of the mode B, W_+, be related to τ as $W_+ = \tau^{-1}e^{-E_i/kT}$. 4) The frequency shift $\delta\omega$ arises principally from terms of the anharmonic vibrational potential of the form $Q_A^2Q_B^2$ (see ref. 3), and may assume a positive or negative value depending on whether the intramolecular interaction of the two modes is repulsive or attractive.

If the simple four-level exchange model, as outlined above, describes the dominant mechanism for affecting the lineshape, we predict that in the low temperature limit the lineshape should behave as eqns (1-3). Note that if one divides the additional linewidth term in eqn. 3 by the frequency shift, a temperature independent constant, $\delta\omega\tau$, is predicted by this theory. The value of this unitless quantity, $\delta\omega\tau$, parameterizes the "regime" of exchange; $|\delta\omega\tau|<1$ is characteristic of fast exchange while $|\delta\omega\tau|>1$ and $|\delta\omega\tau|\sim1$ are associated with slow and intermediate exchange respectively.

B. Interacting Fundamentals ((AO) Exchange)

Abbott and Oxtoby[31] (AO) discuss a different type of exchange process, illustrated for the simplest case in Figure 2. In this model, the modes A

and B are fundamentals lying close in energy, with an energy splitting of $\delta\omega$. As in HSC exchange theory above, it is assumed that the thermal activation of a low-frequency mode causes the dephasing, but here fluctuating anharmonic terms of the form:

$$V_{anh} = f_{iiAB}(t)Q_i^2Q_AQ_B + f_{AB}(t)Q_AQ_B \quad (4)$$

provide the coupling, where A and B are fundamentals and i denotes a low-frequency mode.

The AO approach is similar to the formalism of Nitzen and Silbey[34] where the equation of motion for the matrix elements of the vibrational "superoperator" is obtained to second order in a cumulant expansion. As in the HSC case, the Markov approximation is invoked. From this model, expressions for the frequency shifts and linewidths as a function of temperature are obtained which bear formal similarity to eqns. (2) and (3) but have different physical interpretations. Assuming $\langle Q_i^2 \rangle$ and $\langle Q_i^4 \rangle \propto e^{-E_i/kT}$, the shift and broadening are given by:

$$\text{Shift} = A\delta\omega\tau^2 e^{-E_i/kT}/[1 + \delta\omega^2\tau^2] \quad (5)$$

$$\text{Width} = A\tau e^{-E_i/kT}/[1 + \delta\omega^2\tau^2] \quad (6)$$

Now τ is the decay time of the fluctuating perturbation autocorrelation function of the form:

$$\langle F_{iiAB}(t)F_{iiAB}(o)\rangle \propto \exp(-t/\tau) \quad (7)$$

where it is assumed that all the relevant decay times are the same in order to obtain the simple expressions eqns. (5) and (6). Note that all the

time dependence is included in F and not in Q_i^2.

Thus this theory, like HSC exchange theory, predicts (in the selective coupling cases of Figures 1 and 2) an exponential temperature dependence for the broadening and shift with an activation energy equal to the energy of some low frequency mode. The following predictions also result: 1) In the specific example of Figure 2, the two isolated fundamentals A and B should shift toward each other and display the same E_i as the temperature is increased. 2) τ is the bath correlation time for the anharmonic force, and is typically 0.1-1.0 psec. It should also be mentioned in passing that the presence of the factor A in eqns. (5) and (6) makes it impossible to extract the parameters of interest, namely $\delta\omega$ and τ, as can be done in the HSC exchange model.

C. Dynamic Coupling Model (DC)

In a recent series of papers, Kerthcimer[29,30] has developed a general theory of vibrational dephasing in condensed media based on the Zwanzig-Mori[36] formalism. This theory illustrates the contributions of several mechanisms to the overall dephasing of a given transition, including the exchange processes of Sections A and B. The effects of various energy relaxation and redistribution processes, as well as cross-correlation effects, are taken into account. As was pointed out in reference 30, the HSC exchange model of Section A emerges as a restricted case of the dynamic coupling theory. In the Appendix we discuss the nature of the approximations necessary to reduce the more general theory to this special case, and suggest how the validity of these approximations can be tested experimentally. As the Appendix shows, the general form of the DC theory introduces a dephasing mechanism based on the presence of a dispersive frequency shift τ'^{-1}, which results from the decay of the low-frequency modes into the

bath. This dispersive shift effectively brings nearly into resonance a fundamental and its anharmonically shifted hotband. This results in the transfer of energy as well as phase information, and if this transfer occurs rapidly enough then one must consider the collective vibrational correlation function[30] for all the modes. The importance of this contribution relative to the HSC exchange contribution depends sensitively upon the magnitudes of the various parameters, which are difficult to measure or estimate. Nevertheless, the line-shift and broadening should exhibit approximately Arrhenius temperature dependence, and coupling of a high frequency mode to a specific low frequency mode will often be observed, but the presence of additional unknown parameters makes the extraction of information from experimental data difficult.

D. Experimental Distinction Among Dephasing Models

A careful consideration of the three theoretical models above suggests what experimental procedures may be employed to assess their relative applicability. In their simplest cases, the theories all predict an (approximately) exponential temperature dependence, a strong coupling to a single low-frequency mode, and an equal "activation energy" for the broadening and the frequency shift. They differ, however, in explaining the observed coupling of high and low frequency modes, and in the meanings of the frequency shift and time parameters. In Table I we have summarized briefly the various predictions of each model, and these are illustrated in Figure 3. In this section, we discuss how the differences between the theories can be related to the experiments we have performed.

In the HSC model, coupling between high-frequency and low-frequency modes is thought to result from steric interactions.[3] Therefore, we would

predict that isotopic substitution should not change the mode coupling scheme, i.e., a high-frequency mode should couple to the same low-frequency mode in both the protonated and deuterated molecules. The quantity τ, which can be regarded as a resident lifetime for the low-frequency vibration, should show a concentration dependence that can be interpreted on the basis of resonant energy transfer models. The four-level exchange scheme predicts the presence of a combination level at $\omega_1 + \omega_2 + \delta\omega$ (see Fig. 4). Since $\delta\omega$ is extracted from the analysis of the temperature-dependent lineshape, it is possible to compare experimental combination band frequencies with exchange theory calculated frequencies. Finally, the ratio of the width to the shift at a given temperature, for <u>all</u> modes studied, should yield a temperature-independent quantity approximately equal to one.

In the AO model, two fundamentals will interact if they lie close together in frequency. Since the frequency spacing of the C-H stretches in h_{14}-durene is considerably different than the C-D stretches in d_{14}-durene, the coupling scheme may differ between the two molecules if the AO theory is correct. In either molecule, however, two isolated fundamentals are predicted to shift toward each other with increasing temperature. Also, since the quantity τ in the AO theory is a bath correlation time, it would be expected to show at most a weak concentration dependence.

In the DC model, couplings between modes result from a near resonance between the dispersive and the anharmonic frequency shift. Since such a resonance effect is strongly affected by small changes in either parameter, the coupling schemes in the protonated and deuterated molecules may be considerably different. The direction of shift of a given fundamental may be different in the two isotopic forms, and the ratio of the broadening

to the shift is not expected to be independent of temperature (see Appendix). The time parameter here is essentially the same as in the HSC model, but the anharmonic shifts are expected to be small and positive (5-10 cm^{-1}). This latter prediction can be tested by observing the combination band spectrum.

III. Experimental

Five samples of polycrystalline durene were prepared with various isotopic compositions: pure h_{14}, pure d_{14}, and three mixed samples with 50% d_{14}, 25% d_{14}, and 10% d_{14} in h_{14}. The samples were placed in an Air Products portable helium dewar, which could be varied in temperature from approximately 10°K to room temperature. The temperature was measured by a Chromel vs. Gold thermocouple referenced to ice water, which allowed temperature determination to within ±1°K over most of the temperature range studied (slightly larger errors occur at the lowest temperatures).

The isotropic Raman spectra of the above samples were obtained in the region of interest using a Coherent CR2 Argon laser in conjunction with a Jobin-Yvon Ramanor H525 Raman spectrophotometer. The resolution of 1.0 cm^{-1} was adequate for these studies. Experimental spectra from a chart recorder were subsequently digitized using a Tektronics 4662 Digital Plotter, and computer lineshape analysis was performed in those cases where overlapping occurred between neighboring bands. In this way, accurate values for the linewidths and peak frequencies as a function of temperature were obtained, and were then used to extract the exchange theory parameters using a least-squares fitting procedure as discussed in reference 2.

IV. Results and Discussion

We previously[1,2] reported our analysis of the temperature-dependent Raman spectrum of the C-H stretch region of h_{14}-durene. The results of that analysis are reproduced in Table 2, and were obtained by fitting the experimental data to the lineshape expression given in reference 3. As can be seen from Fig. 5, the Raman spectrum of d_{14}-durene in the C-D stretch region also exhibits the broadening and shifting with temperature that is characteristic of exchange, and can therefore be analyzed in the same way. For this purpose, the spectrum was measured at 10 temperatures from 10°K to room temperature, and the resulting parameters obtained from the fitting process are presented in Table 3.

An important piece of evidence for the applicability of any of the three models of Section II is the match between the "activation energies" listed in Table 3 and the known energies of the low-frequency modes of the molecule. As the Table indicates, in five of seven cases, the observed activation energy corresponds to the energy of a low-frequency fundamental. In the other two cases, the activation energy corresponds to the energy expected for a Raman-inactive combination band (116 cm^{-1} torsion plus 83.5 cm^{-1} libration).[36] This agrees generally with our earlier results on h_{14}-durene.

Evidence in support of HSC exchange is obtained from the dimensionless quantity $\delta\omega\tau$, which is plotted in Figure 6 for the transitions studied in d_{14}-durene. As in the case of h_{14}-durene,[1,2] $\delta\omega\tau$ is approximately unity (intermediate exchange) and is independent of temperature within experimental error. The dynamic coupling model does not, in general, predict temperature independence for this parameter, while the HSC exchange model does assume that both τ and $\delta\omega$ are constant over the temperature region

of interest.

The foregoing results could also be explained on the basis of the AO exchange model. However, the data presented in Fig. 7 contradict the prediction of AO exchange that two well-separated fundamentals must shift <u>together</u> with increasing temperature. The figure shows two bands from the spectrum of d_{14}-durene; there are no Raman peaks within 100 cm^{-1} on the high-frequency side nor within several 100 cm^{-1} on the low-frequency side. Yet the figure shows that these two peaks shift <u>apart</u> with increasing temperature. This could be explained by the AO model only if coupling occurs between the observed Raman peaks and some Raman-inactive transitions nearby. We have examined the IR spectrum of d_{14}-durene in this region and found only a single peak at 2060 cm^{-1}, and no others for at least 60 cm^{-1} in either direction, which indicates that the AO model cannot account for the observed frequency shifts in Fig. 7.

A further experimental test has been carried out based on a major point of distinction between HSC exchange and the DC theory, namely, the energy-level schemes used to explain the dephasing. The HSC theory predicts the presence of combination levels which are anharmonically shifted by $\delta\omega$, whereas the DC theory predicts that the anharmonic shifts should be small and positive ($\sim$5 cm^{-1}). The observation of these combination bands spectroscopically therefore constitutes a crucial test of these two models. Using Fourier Transform Infrared Spectroscopy, we have successfully observed these weak bands with adequate (1 cm^{-1}) resolution, and these spectra for a thin crystal of h_{14}-durene and for d_{14}-durene in KBr are plotted in Figs. 8 and 9 respectively. The arrows on the graph indicate the peak positions predicted on the basis of exchange theory. No predictions are made for the following modes: the 2957.7 cm^{-1} mode in h_{14}-durene, which

has an activation energy that does not match with a low-frequency mode; the modes at 2250.1 cm^{-1} and 2238.9 cm^{-1} in d_{14}-durene, which are overlapping and for which it was therefore difficult to get accurate data; and the 2191.1 cm^{-1} mode in d_{14}-durene, which appears to be a special case and will be discussed below in detail.

Several points should be borne in mind concerning the combination band spectra. First, the combination levels will themselves be expected to show a temperature dependence, and since the spectra were obtained at room temperature, the peaks are shifted in frequency from their zero-temperature positions by an unknown amount. Second, the spectrum of d_{14}-durene was measured in KBr, which contributes a matrix shift to the observed peak positions. Third, the spectrum of h_{14}-durene in the region of interest contains a number of overlapping bands, which make accurate peak position determination difficult in some cases. We estimate that these combined effects introduce an error of 10 cm^{-1} or less in the peak positions. In view of this, the fact that every predicted peak falls within 10 cm^{-1} of an observed peak is strong evidence in favor of our model. The data is particularly convincing in the d_{14} case, since the spectrum is not complicated by extra bands, and the correspondence between the predicted and observed spectra shows up clearly. We believe that this result constitutes a major piece of corroborative evidence for the exchange model.

On the basis of the evidence presented in this section, we feel justified in retaining the simple HSC model for the purpose of analyzing the dynamics of the durene system. We recognize that the AO exchange mechanism and the dynamic coupling mechanism must be included in any complete description of dephasing, however, our aim has been to attempt to

determine the most important dephasing pathways operating in durene. All of the data available can be sufficiently explained using the HSC model.

The chief advantage of the HSC model is that it allows the ready determination of physically meaningful molecular parameters. These parameters are of interest in their own right, but in addition, they can be used to gain insight into those energy transfer and relaxation processes which give rise to the dephasing. In the remainder of this paper, we assume the validity of the HSC exchange model in order to use the information which it yields to gain a deeper understanding of the mechanisms responsible for the dephasing in this system.

V. Mixed Crystal Studies and Interpretation of Results

This section is divided into two parts: in the first, we discuss a steric mechanism for the coupling of high-frequency to low-frequency modes; in the second, we focus on how information from the low-frequency spectrum and from isotopic dilution experiments can be used to characterize the vibrational dynamics. Of particular interest in this connection is the discussion of an exciton model for energy transfer in these low-frequency modes.

A. Steric Interaction of a High-Frequency and a Low-Frequency Mode

In a previous paper,[3] it was concluded that an anharmonic term of the form $C_{AABB}Q_A^2Q_B^2$ (where Q_A and Q_B are vibrational normal coordinates) is chiefly responsible for the coupling which produces the anharmonic shift $\delta\omega$. One possible physical basis for this, as discussed in reference 3, is a steric interaction between the moving atoms of the modes in question. This served as an adequate explanation for several of the observed couplings

in h_{14}-durene, and also can be applied to d_{14}-durene with success, although in both cases the arguments are hampered by the lack of a full assignment of the spectrum in the C-H or C-D stretch regions.

Isotopic dilution experiments carried out on d_{14}-durene have provided a striking piece of evidence in favor of the assumption that, at least in some cases, steric effects are responsible for the observed couplings. Fig. 10 presents the exchange parameters as a function of concentration for the 2191.1 cm^{-1} C-D stretch of d_{14}-durene, which is coupled to the methyl rock at 240 cm^{-1}. Both E_i and τ change significantly with concentration, which is not the case with any other mode studied. At the highest dilution (10% d_{14}), E_i takes on the value of the methyl rock in h_{14}-durene (282 cm^{-1}), and τ takes on the value measured for the methyl rock by the analysis of the 2970.3 cm^{-1} mode in h_{14}-durene (see Table 2). This suggests that this high frequency C-D mode is coupled anharmonically to the methyl rocking mode on an adjacent molecule so that the exchange parameters measured characterize the molecule adjacent to the one being observed. In a highly dilute sample of d_{14}, the adjacent molecules are primarily h_{14}, so E_i and τ approach their values for h_{14}-durene as dilution increases. Figure 10 shows the crystal structure of durene, and illustrates how this proposed intermolecular steric interaction takes place. It can reasonably be assumed that the 2970.3 cm^{-1} mode in h_{14}-durene is coupled by a similar mechanism, and that a general understanding of the nature of the steric couplings in a given molecule may require knowledge of the crystal structure as well as the geometry of the isolated molecule.

B. Low-Frequency Spectra and the Exciton Model

In carrying out an exchange analysis, it is obviously necessary to know the energies of the low-frequency modes of the molecule. In some cases, additional information can be obtained from a careful spectral study of this frequency region as a function of temperature and concentration.

The first example is shown in Fig. 11, which shows the spectrum of a mixed crystal in the region of the CH_3 and CD_3 in plane methyl rocks. In h_{14}-durene, there are two modes coupled to the methyl rock, and in d_{14}-durene, there are three modes coupled to this motion. However, in each molecule two different values of τ are observed for this mode. This apparent contradiction[31] is resolved by the data, since in both molecules the methyl rock transition is clearly split into two components at the lowest temperature. Previous work in h_{14}-durene[40,41] has treated the peaks around 281 cm^{-1} as one band. The possibility that the two peaks represent a Davydov splitting of a single transition can be ruled out, since the splitting is independent of isotopic dilution, and the higher-energy peak does not "borrow" intensity from the lower-energy one with increasing temperature. It is safe to conclude that Fig. 11 illustrates two symmetry modes for the methyl rock, and that the two modes have different τ's. This conclusion is summarized in Figure 12.

A more important question concerns the dynamics of the energy transfer in the low-frequency modes. On the basis of the observed Raman linewidths of these modes, their dephasing times can be calculated. These dephasing times are tabulated in column 6 of Table 3 and are, in several cases, longer than the measured value of τ by up to a factor of ten.[31] This implies that some process which contributes to τ does <u>not</u> contribute to the linewidth; we postulate that this process is coherent, resonant energy transfer

of low-frequency vibrational quanta. In a manner analogous to that of reference 30, we separate the two contributions to τ into a resonant and a relaxation term:

$$1/\tau = 1/\tau_{res} + 1/\tau_{rel} \tag{5}$$

Using the measured values for τ from the exchange analysis, and approximating τ_{rel} by the dephasing time obtained from the appropriate low-frequency mode linewidth, we can obtain an estimate for τ_{res}^{-1}, the resonant energy transfer rate. If this transfer rate exceeds the relaxation rate, a given excitation can traverse more than one molecule in its lifetime, and can properly be described as being partially delocalized or "excitonic" in character. Exciton models developed previously for electronic triplet state excitons in molecular crystals[37-39] can be used as a context for the discussion and analysis of these "vibrational excitons."[42,43] We present here only a simple outline of a vibrational exciton model, in order to illustrate the possibilities inherent in such a concept. It is not to be expected that a complete understanding of vibrational excitonic properties will be realized here, but it will be demonstrated that a useful and interesting semiquantitative picture can be obtained from the data in a straightforward way.

An examination of the low-frequency linewidths, in conjunction with the values of τ obtained from the exchange analysis, can yield an indication of the degree of delocalization present in each low-frequency mode. We define a quantity $\langle n \rangle$, the average number of coherent jumps for a given mode:

$$\langle n \rangle = \frac{\tau_{rel}}{\tau} \tag{6}$$

This quantity is tabulated in column 7 of Table 3, and it can be seen that the largest values of <n> occur for the modes at 2191.1 cm^{-1} and 2225.9 cm^{-1}, which are both coupled to the A_g methyl rock motion at 240 cm^{-1}. In agreement with reference 36, we advance the assumption that this methyl rock exhibits significant excitonic character, and present the results of an investigation of this hypothesis. This investigation has relied upon direct observation of the Raman spectrum of the methyl rock as a function of temperature and concentration, and also indirect observation through exchange analysis of the coupled high-frequency mode at 2225.9 cm^{-1}.

The concentration dependence of the low-temperature spectrum of the methyl rock in both d_{14}-durene and h_{14}-durene is given in Table 4. The important point to note is that as each pure species is substituted with its isotopic analog, the methyl rock peak shifts to lower frequency by approximately 3 cm^{-1}. This can be explained readily within the framework of the vibrational exciton picture, in which the exciton $\vec{k}$ states are a band of linear combinations of isolated molecular states. In a pure crystal, the location of the spectroscopically allowed ($\vec{k} = 0$) transition within this band of states determines the observed peak frequency. The observed frequency in a dilute species, on the other hand, is simply the transition frequency of the isolated molecule, since resonant energy transfer is forbidden and the exciton picture is invalid. The data of Table 4 therefore implies that, in the pure crystal, the transition frequency of $\vec{k} = 0$ is raised approximately 3 cm^{-1} above the transition frequency of the isolated molecule, and hence the full width of the exciton band is approximately 6 cm^{-1}. It should be mentioned that the data cannot be accounted for by assuming that the frequency shift results from a change in intermolecular potential upon isotopic substitution, since both peaks shift in

the same direction with dilution.

Further evidence for the validity of the exciton picture emerges from a consideration of the temperature dependence of the linewidth of the d_{14}-durene methyl rock, shown in Table 5. It is known from studies of electronic exciton spectra[37] that, at elevated temperatures, phonon scattering serves to localize the excitations. In effect, this results in the redistribution of oscillator strength into exciton states other than $\vec{k} = 0$, and consequently as the temperature is increased, the linewidth broadens to reflect the entire range of $\vec{k}$ states comprising the exciton band.[37,38] This explains the behavior observed in d_{14}-durene, where the methyl rock broadens from 4.0 cm^{-1} at low temperature to 6.2 cm^{-1} at 275°K, in agreement with our estimate of 6 cm^{-1} for the exciton bandwidth.

Although this evidence is consistently in support of the proposed exciton picture, a more crucial test of this hypothesis lies in its ability to explain the observed behavior of τ as a function of concentration. To model the concentration dependence, we assume that the relaxation time for decay of low-frequency modes into lattice modes (τ_{rel} in Equation 5) is independent of concentration. This assumption is equivalent to asserting that for lattice modes, the difference in frequency between a given d_{14}-durene mode and the corresponding h_{14}-durene mode is less than the linewidths of those modes, or in other words, the trap depth for lattice modes is less than their bandwidth (the amalgamation limit).[36,39] Conversely, the resonant energy transfer time (τ_{res} in Equation 5) may be concentration dependent, since from Fig. 11 the lineshapes of the methyl rock in the two isotopic species are well separated. If the molecule under observation is present in a concentration c, its effective τ_{res} will be a function of the concentration and the pure crystal resonant transfer time, $\tau_{res,pure}$:

$$1/\tau_{res} = \alpha(c)1/\tau_{res,pure} \tag{7}$$

Substitution of (7) into Equation (5) now gives:

$$\frac{1}{\tau} = \alpha(c)\left[\frac{1}{\tau_{res,pure}}\right] + \frac{1}{\tau_{rel}} \tag{8}$$

The function $\alpha(c)$ characterizes the type of energy transfer: in a localized, non-excitonic picture, where nearest neighbor interactions are important, $\alpha(c)$ decreases smoothly from $\alpha(c) = 1$ at $c = 1$ to $\alpha(c) = 0$ at $c = 0$; in a delocalized, excitonic picture, where resonant interactions extend over several lattice sites, $\alpha(c)$ remains constant from $c = 1$ down to some critical concentration (typically 10%), below which Anderson localization takes place.[39] Thus, if τ increases with dilution, it indicates non-excitonic behavior, while a constant τ is indicative of exciton behavior.

Examples of both were observed in our series of mixed crystal studies, and the data for one of each type is given in Table 6. In agreement with our expectations concerning the A_g methyl rock, τ for the coupled high-frequency mode at 2225 cm^{-1} remains constant as a function of dilution. This behavior, taken with the other available evidence, provides justification for the use of the exciton model in describing the dynamics of this mode.

A different trend appears in the data from the 2035 cm^{-1} mode, which is coupled to the B_{1g} methyl rock. In this case, τ lengthens by a factor of 2 over the concentration range studied, as given in Table 6 and shown graphically in Fig. 13. By a simple linear extrapolation of the data, we estimate τ_{rel}, the relaxation time into lattice modes for the B_{1g} methyl rock, to be 1.4 ± .1 psec, and the energy transfer time, τ_{res}, to be 1.2 ± .1 psec. The value of τ_{rel} obtained in this way differs by less than a

factor of two from the inverse linewidth of this mode. Based on these values, we conclude that the exchange mechanism for this mode consists of excitations and de-excitations of isolated molecules.

The results of the foregoing analysis lend new insight into the detailed nature of the exchange process. They illustrate how spectral evidence of various kinds may be used to characterize the exchange mechanism in terms of its localized or delocalized nature, and how the linewidth of a low frequency mode, together with exchange analysis of the coupled high-frequency modes, can be used to provide a direct measure of the degree of excitonic character present in that low-frequency mode. The data suggests that, in this molecule, different degrees of delocalization occur for different low-frequency modes, but that the concept of a delocalized vibrational exciton must not be neglected in modeling the dynamical behavior of vibrations in molecular solids.

VI. Conclusion

The results presented here on d_{14}-durene, along with the earlier work on h_{14}-durene, provide strong evidence for the utility of the simple exchange model. The presence of intermediate exchange and the excellent correspondence between calculated activation energies and known energies of low-frequency modes constitute important support for the exchange model. Of particular interest is the successful observation by infrared spectroscopy of the combination bands predicted by exchange theory. This latter result, along with qualitative observations of the temperature-dependent frequency shifts in these molecules, tends to corroborate exchange theory in preference to other proposed models.

The results of the exchange theory analysis applied to high-frequency modes, plus measurements of the linewidths of the coupled low-frequency modes, have led to the conclusion that the low frequency methyl group modes of these molecules exhibit significant delocalized or "excitonic" character. The assumption of exciton behavior not only explains the observed low-frequency mode linewidths, but also enables a series of mixed crystal studies to yield insight into the relative importance of resonant and non-resonant energy transfer processes in the exchange mechanism.

The use of exchange theory to interpret this simple series of experiments has resulted in a detailed understanding of the dynamics of this system. Further applications of this theory to other such systems and, in particular, to the problem of vibrational dephasing in liquids is currently in progress.[32]

Appendix

In the Zwanzig-Mori formalism, the motion of a dynamical variable A is described by an equation of the form[30]

$$\frac{d}{dt}A(t) - i\omega_o A(t) = \int_0^t \phi(t-s)A(s)ds + f(t) \qquad (A.1)$$

where ω is the frequency, $f(t)$ is a random force acting upon A, and ϕ is a damping function related to $f(t)$ by the fluctuation-dissipation theorem:

$$\phi(t) = \langle f(t)f^*(o)\rangle \qquad (A.2)$$

The brackets represent ensemble averages. In order to describe the motion of more than one dynamical variable, equation (A.1) can be regarded as a matrix equation. The solution of (A.1) is

$$A(t) = \Xi(t)A(o) + \int_0^t \Xi(t-s)\cdot f(s)d.s \qquad (A.3)$$

where the correlation function $\Xi(t)$ is defined in terms of its Fourier transform:

$$\Xi(\omega) = \frac{1}{\omega 1 - \omega_o - i\hat{\phi}(\omega)} \qquad (A.4)$$

and

$$\hat{\phi}(\omega) = \int_0^\infty \exp(-i\omega t)\phi(t)dt \qquad (A.5)$$

The problem is reduced to the evaluation of $\phi(\omega)$ according to (A.2), i.e., finding the Fourier transforms of the force autocorrelation functions. This is the approach employed by Wertheimer[29,30] in treating vibrational dephasing in condensed systems.

The form of (A.4) requires an approximation to be made in the case where the quantities A, ϕ, f, and ω_o are matrices, namely, the matrix ϕ must be diagonalized. This is accomplished using Rayleigh-Schroedinger perterbation theory, which results in new matrix elements ϕ_i' given by

$$\phi_i' = \phi_{ii} + \sum_{i=j} \frac{\phi_{ij}\phi_{ji}}{\phi_{ii} - \phi_{jj}} \qquad (A.6)$$

where $\phi_{ij}(t) = \langle f_i(t)f_j^*(o)\rangle$ and $f_i(t)$ is the random force on dynamical variable A_i.

In the Markoff approximation, it is assumed that $\phi_{ij}(t)$ = constant $x\delta(t)$ and hence $\phi_{ij}(\omega)$ = constant. The exchange theory of Harris[3] can be readily derived by considering two modes: A_1 with resonance frequency ω_o, and A_2 with resonance frequency $\omega_o + \Delta\omega$. The quantity τ characterizes

the linewidth in the absence of dephasing, τ^{-1} is the depopulation rate of mode 2, and the quantity $\sigma = \exp(-E_i/kT)$ is introduced in the ensemble averaging process to satisfy detailed balance:

$$\phi_{11}(\omega) = T + \sigma\tau^{-1} \tag{A.7a}$$

$$\phi_{22}(\omega) = T + \tau^{-1} \tag{A.7b}$$

$$\phi_{21}(\omega) = \sigma\tau^{-1} \tag{A.7c}$$

$$\phi_{12}(\omega) = \tau^{-1} \tag{A.7d}$$

$$\omega_{11} = \omega_0 \tag{A.7e}$$

$$\omega_{22} = \omega_0 + \Delta\omega \tag{A.7f}$$

Combination of (A.7) with (A.6) and (A.4) gives, in the low temperature limit $\sigma \ll 1$:

$$R(\omega) = \frac{1}{\omega I - L} \tag{A.8}$$

where the matrix L is diagonal. The lineshape of the transition A_1 can be described by calculating L_1:

$$L_1 \text{ (exchange)} = \omega_0 + T - i\sigma \frac{\Delta\omega\tau^{-1}}{i\Delta\omega + \tau^{-1}} \tag{A.9}$$

Using the fact that Re(L) = frequency and Im(L) = damping, we obtain

$$\text{Re}(L) = \omega_{eff} = \omega_0 + \frac{\sigma\tau^2(\Delta\omega)^2}{1 + (\Delta\omega)^2\tau^2} \tag{A.10}$$

$$\text{Im}(L) = T_{eff} = T + \frac{\sigma\tau\Delta\omega}{1 + (\Delta\omega)^2\tau^2} \tag{A.11}$$

which are the same as reference 3.

A more careful and comprehensive development along these lines sheds further light on the meaning of the parameters in (A.10) and (A.11), and allows the inclusion of additional dephasing and relaxation mechanisms. This more careful approach differs from the derivation above in three important respects: 1) The presence of more than one pair of exchanging modes can be readily represented. 2) Additional dephasing mechanisms are included by adding more terms to the force autocorrelation functions (A.2). Any physical process whose contribution is to be considered can be described by choosing an appropriate functional form for $\phi(t)$. 3) The Markoffian approximation need not be invoked; instead, Wertheimer employs a "quasi-Markoffian" approximation[30] in which $\phi(\omega)$ is a complex constant ϕ_a near a resonance of interest $\omega = \omega_a$. In other words, $\phi(\omega)$ is still considered to be a constant, as in the Markoffian case, but the value of the constant depends upon the frequency of a nearby resonance ω_a.

The treatment of reference 30 includes the effects of exciton transfer processes in both the low-frequency and high-frequency modes, the effects of dynamic coupling between a given high-frequency mode and neighboring modes (this is particularly important when Fermi resonances are present), the effects of cross-correlations, and the effects of relaxation of the low-frequency modes. It is shown[30] that when only one pair of modes is important, equation (A.9) is still the correct functional form to describe the lineshape, but that the quantities $\Delta\omega$ and τ have imaginary components. The presence of these components, denoted by $\Delta\omega'$ and τ' respectively, produces a dephasing contribution which differs physically from exchange, and is described by

$$L_1(\text{dynamic}) \cong \omega_0 + i\Gamma - \sigma \left[\frac{\tau'^{-1}\Delta\omega}{(\tau'^{-1} - \Delta\omega)^2 + (\tau^{-1} - \Delta\omega')^2}\right]$$

$$X[\tau'^{-1} - \Delta\omega) - i(\tau^{-1} - \Delta\omega')] \qquad \text{(A.12)}$$

Two important conclusions can be drawn from this equation. The first stems from the consideration that τ'^{-1} is, according to the discussion of ref. 29 and 30, temperature-dependent. Since the frequency shift from (A.12) is proportional to $(\tau'^{-1} - \Delta\omega)$, the possibility exists that the direction of the frequency shift could reverse with increasing temperature. We have never observed such behavior experimentally. In any case, the ratio of the broadening to the shift, which is temperature-independent in the HSC model, is not expected to be temperature independent in the dynamic coupling treatment. The second conclusion concerns the coupling of high- to low-frequency modes. From (A.12) we would anticipate that a given high-frequency mode would be coupled most strongly to that low-frequency mode for which the prefactor $\tau^{-1}\Delta\omega/[(\tau'^{-1} - \Delta\omega)^2 + (\tau^{-1} - \Delta\omega')^2]$ is small, which would suggest that $\tau^{-1} \approx \Delta\omega$. However, in the infrared combination band spectra shown in the body of the paper, the positions of the observed peaks seem more consistent with the exchange predictions than with the scheme suggested by (A.12).

The available evidence tends to indicate that the imaginary components of $\delta\omega$ and τ are in fact small, in which case (A.9) retains its usefulness. It should be noted, however, that both of the mechanisms (A.9) and (A.12) will be present to a greater or lesser extent in any given situation, and a choice between them depends on a knowledge or estimate of the parameters involved. It seems desirable, therefore, to retain the exchange model (A.9)

whenever possible, owing to the clear physical interpretation of the parameters $\delta\omega$ and τ.

Acknowledgement

The authors wish to acknowledge fruitful discussion and correspondence with Reiner K. Wertheimer, and the assistance of Linda Young and Richard MacPhail in obtaining the FTIR spectra.

This work was supported in part by the National Science Foundation, and by the Division of Chemical Sciences, Office of Basic Energy Sciences, U. S. Department of Energy, under contract No. W-7405-Eng-48.

References

1. C. B. Harris, R. M. Shelby, and P. A. Cornelius, Phys. Rev. Lett. 38, 1415 (1977).
2. C. B. Harris, R. M. Shelby, and P. A. Cornelius, Chem. Phys. Lett. 57, 8 (1978).
3. R. M. Shelby, C. B. Harris, and P. A. Cornelius, J. Chem. Phys. 70, 34 (1979).
4. A. Laubereau and W. Kaiser, Chemical and Biochemical Applications of Lasers, C. B. Moore, ed. (Acad. Press, 1976).
5. A. Laubereau, G. Wochner, and W. Kaiser, Phys. Rev. A13, 2212 (1976).
6. H. M. McConnell, J. Chem. Phys. 28, 430 (1958).
7. P. W. Anderson, J. Phys. Soc. Jap. 9, 316 (1957).
8. R. Kubo and K. Tomita, J. Phys. Soc. Jap. 9, 888 (1954).
9. C. B. Harris, J. Chem. Phys. 67, 5607 (1977).
10. P. de Bree and Douwe A. Wiersma, private communication (1979).
11. K. Dressler, O. Oehler, and D. A. Smith, Phys. Rev. Lett. 34, 1384 (1975).
12. J. Wiesenfeld and C. B. Moore, Bull. Am. Phys. Soc. 21, 1289 (1976).
13. K. Tanabe and J. Jonas, J. Chem. Phys. 67, 4222 (1977).
14. S. F. Fischer and A. Laubereau, Chem. Phys. Lett. 35, 6 (1975).
15. M. Shugard, J. C. Tully, and A. Nitzan, J. Chem. Phys. 69, 336 (1978).
16. S. Mukamel, Chem. Phys. 31, 327 (1978).
17. S. Mukamel, Chem. Phys. 37, 33 (1979).
18. R. Silbey, Ann. Rev. Phys. Chem. 27, 203 (1976).
19. D. W. Oxtoby and S. A. Rice, Chem. Phys. Lett. 43, 1 (1976).
20. S. Voelker, R. M. Macfarlane, and J. H. van der Waals, Chem. Phys. Lett. 53, 8 (1978).

21. M. N. Sapozhnikov, J. Chem. Phys. 68, 2352 (1978).

22. D. E. McCumber, Phys. Rev. 133A, 163 (1964).

23. A. G. Redfield, Adv. Magn. Res., Vol. I, 1 (1965).

24. F. P. Burke and G. J. Small, J. Chem. Phys. 61, 4588 (1974).

25. S. Lin and H. Eyring, Proc. Natl. Acad. Sci. USA 74, 3623 (1977).

26. H. D. Ladouceur and D. J. Diestler, J. Chem. Phys. 70, 2620 (1979).

27. D. W. Oxtoby, J. Chem. Phys. 70, 2605 (1979).

28. D. W. Oxtoby, Adv. Chem. Phys. 40, 1 (1979).

29. R. K. Wertheimer, Chem. Phys. Lett. 52, 224 (1977); Mol. Phys. 38, 797 (1979); Chem. Phys. 41, 229 (1974).

30. R. K. Wertheimer, Chem. Phys. 45, 415 (1980).

31. R. S. Abbott and D. W. Oxtoby, J. Chem. Phys. 70, 4703 (1979).

32. C. B. Harris, H. Auweter and S. M. George, Phys. Rev. Lett. 44, 737, (1980).

33. A. Laubereau, D. van der Linde, and W. Kaiser, Phys. Rev. Lett. 27, 802 (1971).

34. A. Nitzan and R. J. Silbey, J. Chem. Phys. 60, 407 (1974).

35. H. Mori, Prog. Theor. Phys. 33, 423 (1965).

36. P. N. Prasad and R. Kopelman, J. Chem. Phys. 58, 126 (1973).

37. C. B. Harris and D. A. Zwemer, Ann. Rev. Phys. Chem. 29, 473 (1978).

38. Yutaka Toyozawa, Prog. Theor. Phys. 20, 53 (1958).

39. Y. Onodera and Y. Toyozawa, J. Phys. Soc. Jap. 24, 341 (1968).

40. P. Prasad and R. Kopelman, J. Chem. Phys. 58, 5031 (1973).

41. M. A. Kovner, Opt. Spektrosk. 1, 348 (1956).

42. J. C. Lavfer and R. Kopelman, J. Chem. Phys. 53, 3674 (1970).

43. J. E. Cahill, J. Chem. Phys. 66, 4847 (1977).

Table 1. Vibrational Dephasing Models

	HSC	AO	DC
Temperature Dependence	Width α exp $(-\beta\hbar\omega)$ Shift α exp $(-\beta\hbar\omega)$ ω is frequency of the coupled low-frequency mode.	Same as HSC	Very complicated, but approximately exponential as in HSC
Coupling	Results from anharmonic shift; dominant term is of the general form $Q_A^2 Q_B^2$; suggests steric interaction.	Results from anharmonic term of form $Q_i^2 Q_A Q_B$; no specific interpretation.	Results from accidental equality of dispersive shift and anharmonic shift.
Frequency Shift $\delta\omega$	$\delta\omega$ is anharmonic shift of combination level; may be of either sign	$\delta\omega$ is spacing between two adjacent fundamentals; they must shift together with increasing temperature.	Results from difference between dispersive and anharmonic shifts; may have either sign.
Time Parameter, τ	τ is resident lifetime of vibrational exciton.	τ is both correlation time for anharmonic force constant F_{iAB}.	Decay rates for exciton relaxation processes of all types are explicitly included.

Table 2. Parameters obtained from least-squares analysis of temperature-dependent lineshape data.

	Raman Active C-H Stretch		Low Frequency Dephasing Channels			
	ω_o (cm^{-1})	Mode	Dephasing Mode	ε_i(cm^{-1})	$\delta\omega$(cm^{-1})	τ(ps)
a	2929.0	A_g, B_{1g}	B_{3g} - Torsion	194±10	+13.6	0.36
b	2957.7	A_g, B_{1g}		229±21	+10.5	0.86
c	2970.3		B_{1g}, A_g - Methyl Rock	265±6	-24.2	0.19
d	2987.3	B_{2g}, B_{3g}	B_{3g}, B_{2g} Out-of-plane Methyl Bend	341±13	-20.6	0.25
e	3027.5	A_g	B_{1g}, A_g-Methyl Rock	253±19	-21.2	0.36

Table 3. Exchange Parameters in d_{14}-durene

ω_o (cm^{-1})	E_i (cm^{-1})	Coupled low-frequency mode[e]	$\delta\omega$ (cm^{-1})	τ (psec)	τ_{rel}[a]	<n>
2035.4	252±10	B_{1g} methyl rock	-12.0±.5	.66±.03	2.65	4.02
2049.9	190±12	Inactive combination band[b]	8.8±.4	.77±.06	c)	c)
2191.1	240±20	A_g methyl rock	19.5±1.0	.30±.06	2.65	8.83
2211.6	200±10	Inactive combination band[b]	-11.4±.6	.45±.05	c)	c)
2225.9	240±15	A_g methyl rock	-16.1±.7	.36±.07	2.65	7.36
2250.1[d]	105±10		-4.9±.3	3.1±.3	4.42	1.43
2238.9[d]	90±15		-5.6±.2	4.3±.2	2.52	0.59

a) Calculated from the observed FWHM of the low-frequency Raman spectrum, using $\tau = 1/\pi c(\text{FWHM})$.

b) A frequency of approximately 200 cm^{-1} is expected from a combination of the torsional mode at 116 cm^{-1} and a libration at 83.5 cm^{-1}.[36]

c) The linewidth for the coupled, Raman-inactive combination band is not available.

d) An additional source of error is present in these modes since the lines begin overlap at higher temperatures.

e) The low-frequency vibrational spectrum of d_{14}-durene consists of a methyl rock at 240 cm^{-1}, torsions at 116 cm^{-1} and 140 cm^{-1}, and librations at 83.5 cm^{-1} and 105 cm^{-1}.[36]

Table 4. Concentration Dependence of Ag Methyl Band Lineshapes in h_{14}- and d_{14}-durene.

Environment	100% d_{14}-durene	50% d_{14}-durene 50% h_{14}-durene	25% d_{14}-durene 75% h_{14}-durene	10% d_{14}-durene 90% h_{14}-durene
d_{14}-durene peak position (cm^{-1})	249.2	248.4	247.6	246.6
FWHM (cm^{-1})	4.0	5.2	5.0	4.0
h_{14}-durene peak position		279.4	280.4	280.8
FWHM (cm^{-1})		4.4	3.6	3.6

Table 5. Temperature Dependent Linewidth of Ag Methyl Rock in d_{14}-durene (FWHM in cm^{-1})

10°K	90°	130°	170°	225°	250°	275°
4.0	4.6	4.8	6.0	6.1	6.1	6.2

Table 6. Concentration Dependence of Exchange Parameters of C-D Stretch Modes in d_{14}-durene.

Environment	$\delta\omega$ (cm^{-1})	E_i (cm^{-1})	τ(psec)
2225 cm^{-1} Stretch			
100% d_{14}-durene	-16.1±.7	240±10 (240)	.36±.07
50% d_{14}-durene 50% h_{14}-durene	-15.0±1	250±10 (240)	.35±.07
25% d_{14}-durene 75% h_{14}-durene	-14.1±1	250±10 (240)	.34±.07
2035 cm^{-1} Stretch			
100% d_{14}-durene	-12.0±.5	252±15 (240)	.35±.05
50% d_{14}-durene 50% h_{14}-durene	-10.5±1	211±15 (240)	.9±.05
25% d_{14}-durene 75% h_{14}-durene	-11.0±1	230±15 (240)	1.1±.08
10% d_{14}-durene 90% h_{14}-durene	-12.0±1	235±15 (240)	1.2±.1

FIGURE CAPTIONS

Figure 1. Two anharmonically coupled vibrational modes undergoing energy exchange. The anharmonic coupling produces a frequency shift $\delta\omega$, while thermal fluctuations cause an excitation and de-excitation of the low-frequency mode B.

Figure 2. When two fundamentals differ in frequency by an amount $\delta\omega$, energy exchange between them results in dephasing. The coupling Hamiltonian involves a low-frequency mode with an energy on the order of kT.

Figure 3. The qualitative differences in spectral appearance at low and high temperature are illustrated for the three models: HSC (or hotband) exchange, AO exchange of interacting fundamentals, and the DC (dynamic coupling) model.

Figure 4. Information about coupling of vibrational modes and vibrational dephasing of a given mode can be obtained from three different spectral regions: the fundamental region, where the mode A transition and possibly its hot band can be observed; the low frequency region, where the coupled low-frequency mode B appears; and the combination band, where the peak positions can be used to confirm the presence of coupling of mode A to mode B.

Figure 5. The d_{14}-durene Raman spectrum clearly shows broadenings and shiftings characteristic of exchange. A similar type of behavior in h_{14}-durene can be found in references 1 and 2.

Figure 6. Each point is obtained by dividing the observed broadening by the frequency shift at a given temperature. HSC exchange predicts that the resulting quantity is temperature independent and approximately 1.

Figure 7. A portion of the Raman spectrum of d_{14}-durene at several temperatures. These peaks, which are clearly separated from other modes of the molecule, shift away from each other with increasing temperature, in contradiction to the AO exchange model.

Figure 8. Room-temperature IR spectrum of neat h_{14}-durene in the region where HSC theory predicts the presence of combination bands. Numbers in parenthesis are the positions of peaks predicted on the basis of this theory. In each case, an observed peak is located within 10 cm^{-1} of a predicted peak.

Figure 9. Room-temperature IR spectrum of d_{14}-durene in KBr. Numbers in parenthesis are predicted peaks based on HSC exchange; as in fig. 8, each falls within 10 cm^{-1} of an observed peak.

Figure 10. The crystal structure of durene, showing how steric hindrance between adjacent molecules can occur. This explains the observed behavior of the exchange theory parameters as a function of concentration.

Figure 11. Durene exhibits two Raman-active methyl rocking modes, which are resolved spectroscopically at low temperature, but coalesce by 90°K. In addition, it should be noted that these transitions broaden and shift with increasing temperature, in agreement with the proposed vibrational exciton model.

Figure 12. An illustration of the two methyl rocking motions observed in Figure 11. The different values of τ allow the assignment of the coupling scheme between the methyl rocks and the high-frequency modes.

Figure 13. The data is for the 2035 cm^{-1} mode, which is coupled to the B_{1g} methyl rock. The slope of the line gives an estimate for τ_{res} of 1.2 ± .1 psec; the intercept gives τ_{rel} as 1.4 ± .1 psec. These values suggest that the B_{1g} methyl rock does not exhibit significant excitonic properties.

VIBRATIONAL ENERGY EXCHANGE
BETWEEN ANHARMONICALLY COUPLED STATES

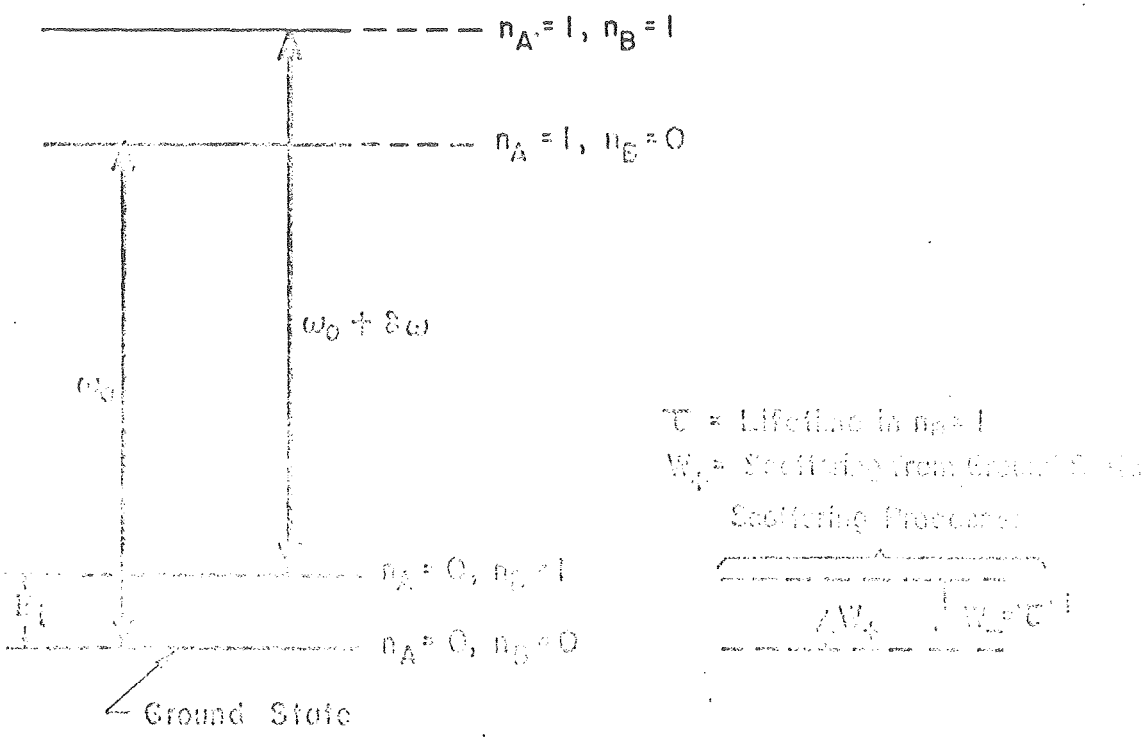

XBL 704-6107

Figure 1

INTERACTING FUNDAMENTALS

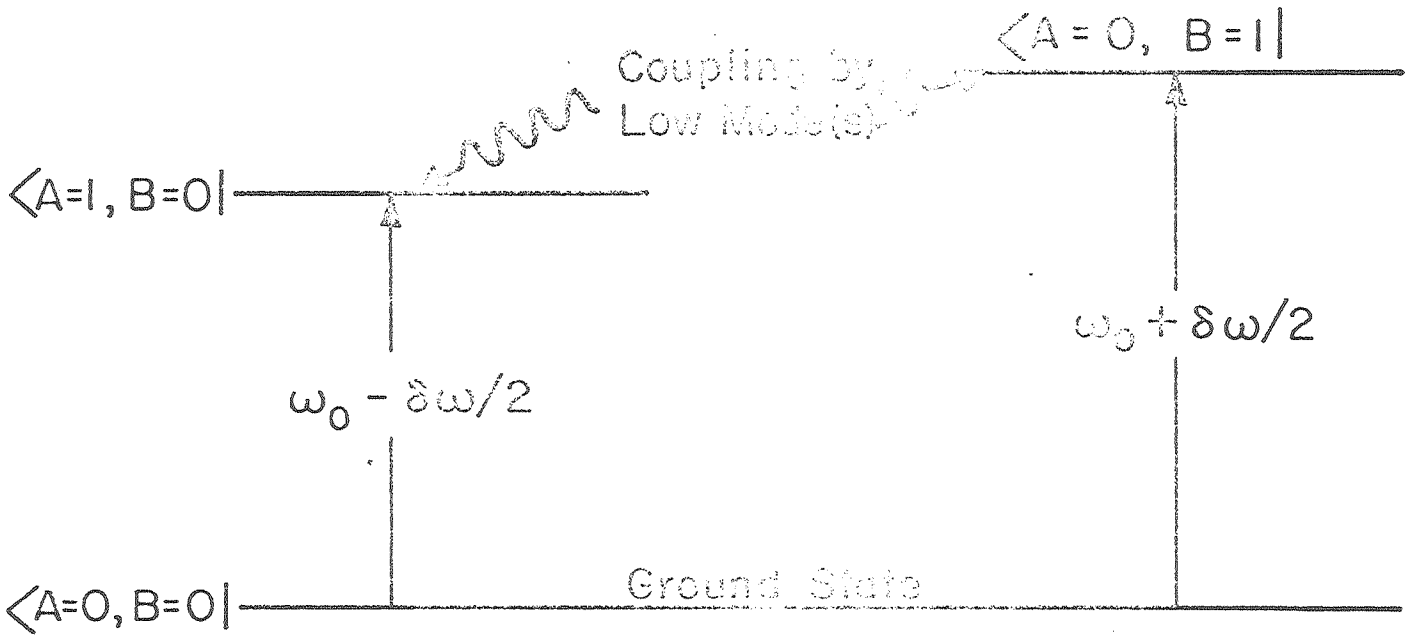

$$V_{coupling} = F_{ABLL}(t)\ \underbrace{q^2_{low}}_{\text{Statistically Weighted}}\ Q_A\ Q_B$$

XBL 7911-7282

Figure 2

A COMPARISON OF VIBRATIONAL DEPHASING MODELS

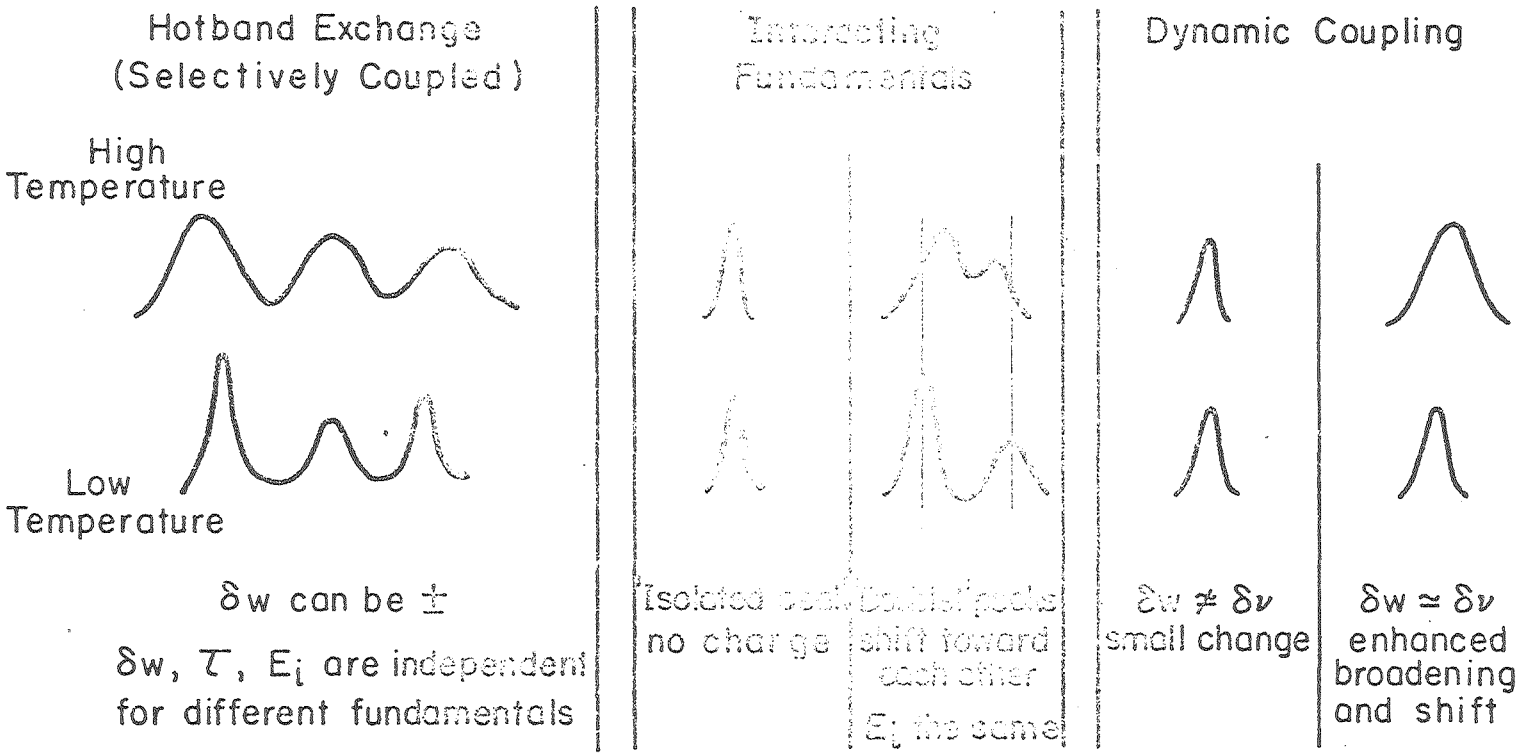

XBL7912-5479

Figure 3

SPECTROSCOPY OF ANHARMONICALLY COUPLED VIBRATIONAL OSCILLATORS

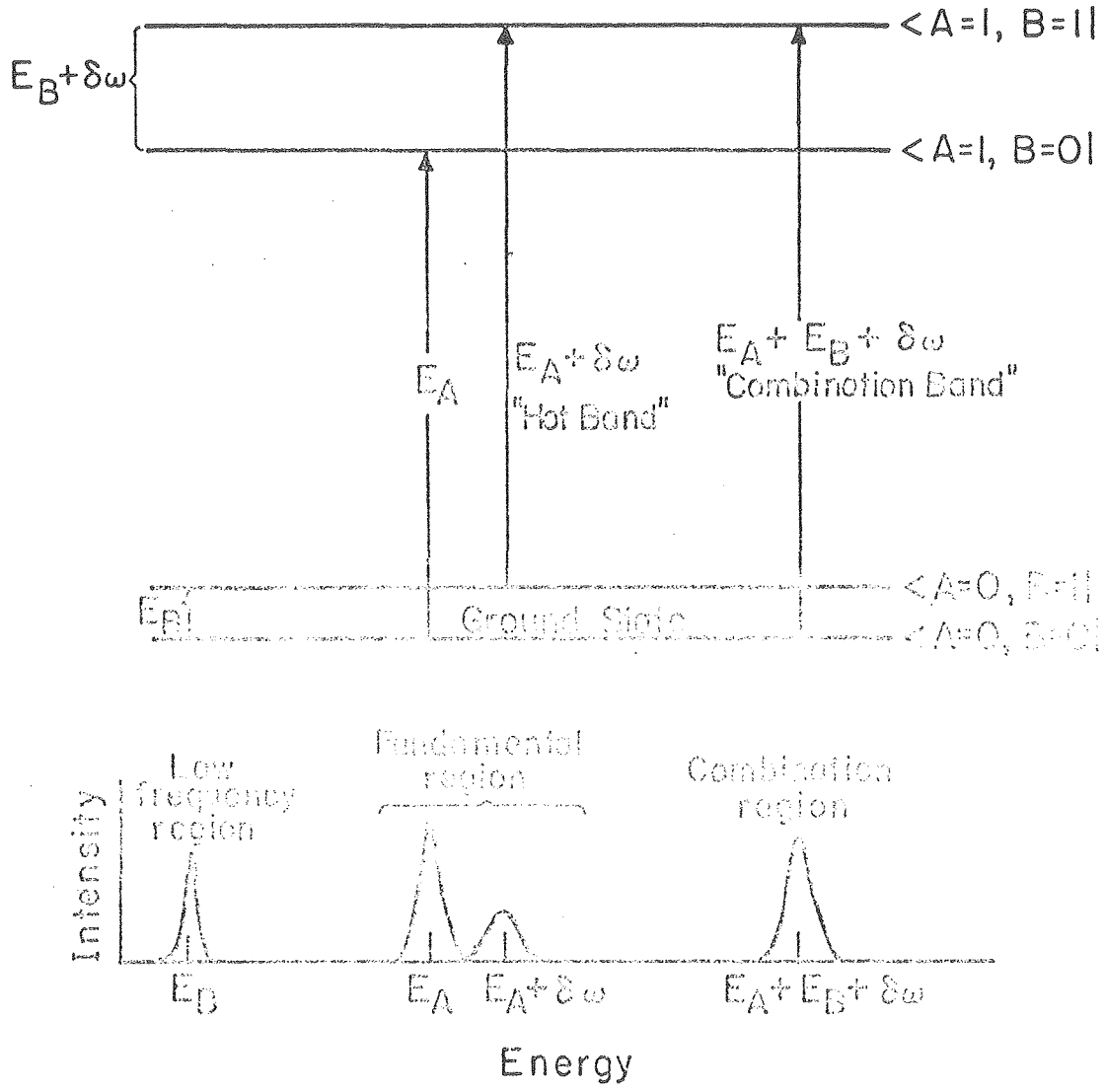

XBL7912-5467

Figure 4

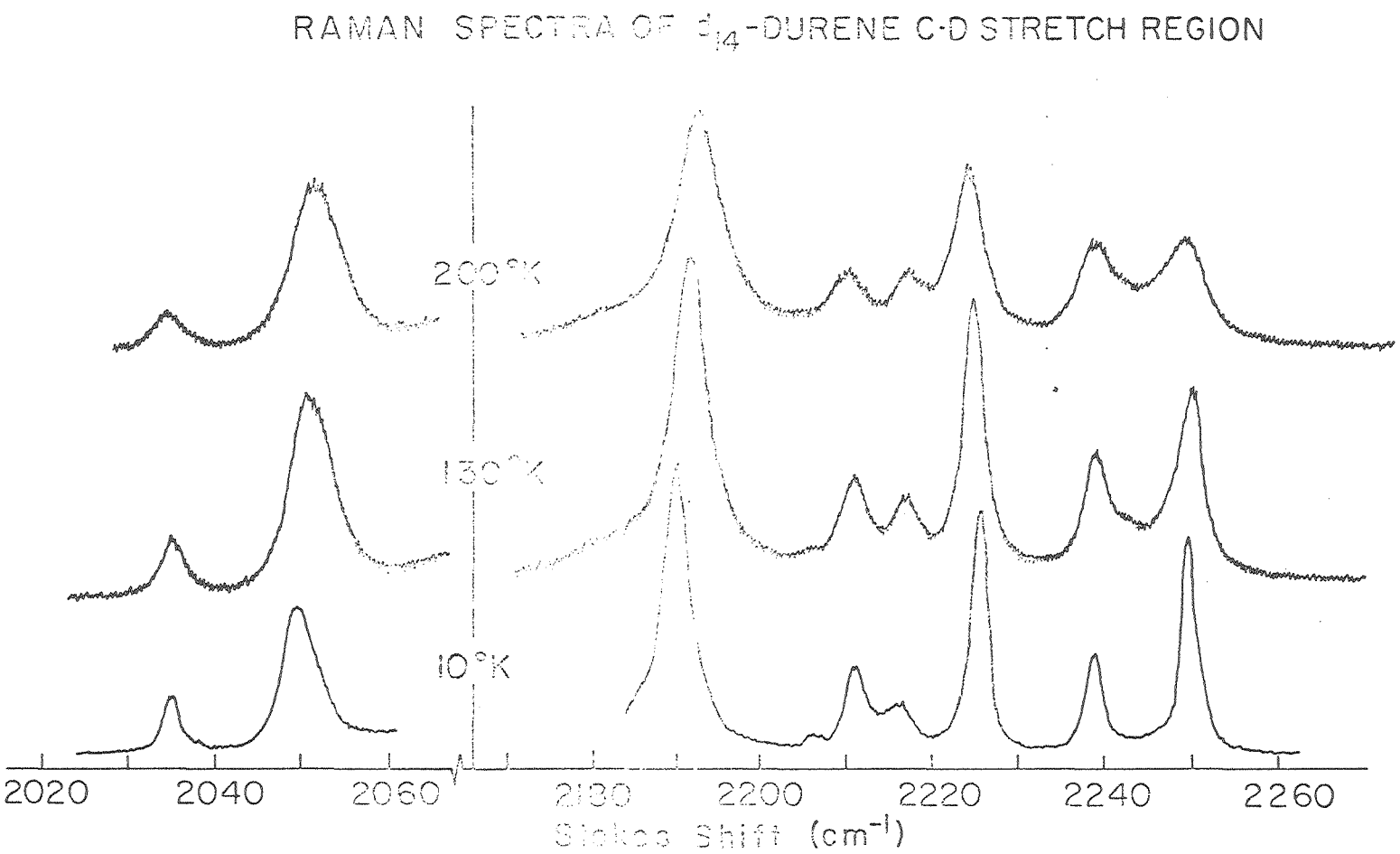
RAMAN SPECTRA OF d_{14}-DURENE C-D STRETCH REGION
200°K
130°K
10°K
2020
2040
2060
2180
2200
2220
2240
2260
Stokes Shift (cm^{-1})
XBL795-6249

Figure 5

RATIO OF LINEBROADENING TO FREQUENCY SHIFT
AS A FUNCTION OF TEMPERATURE IN d_{14}-DURENE

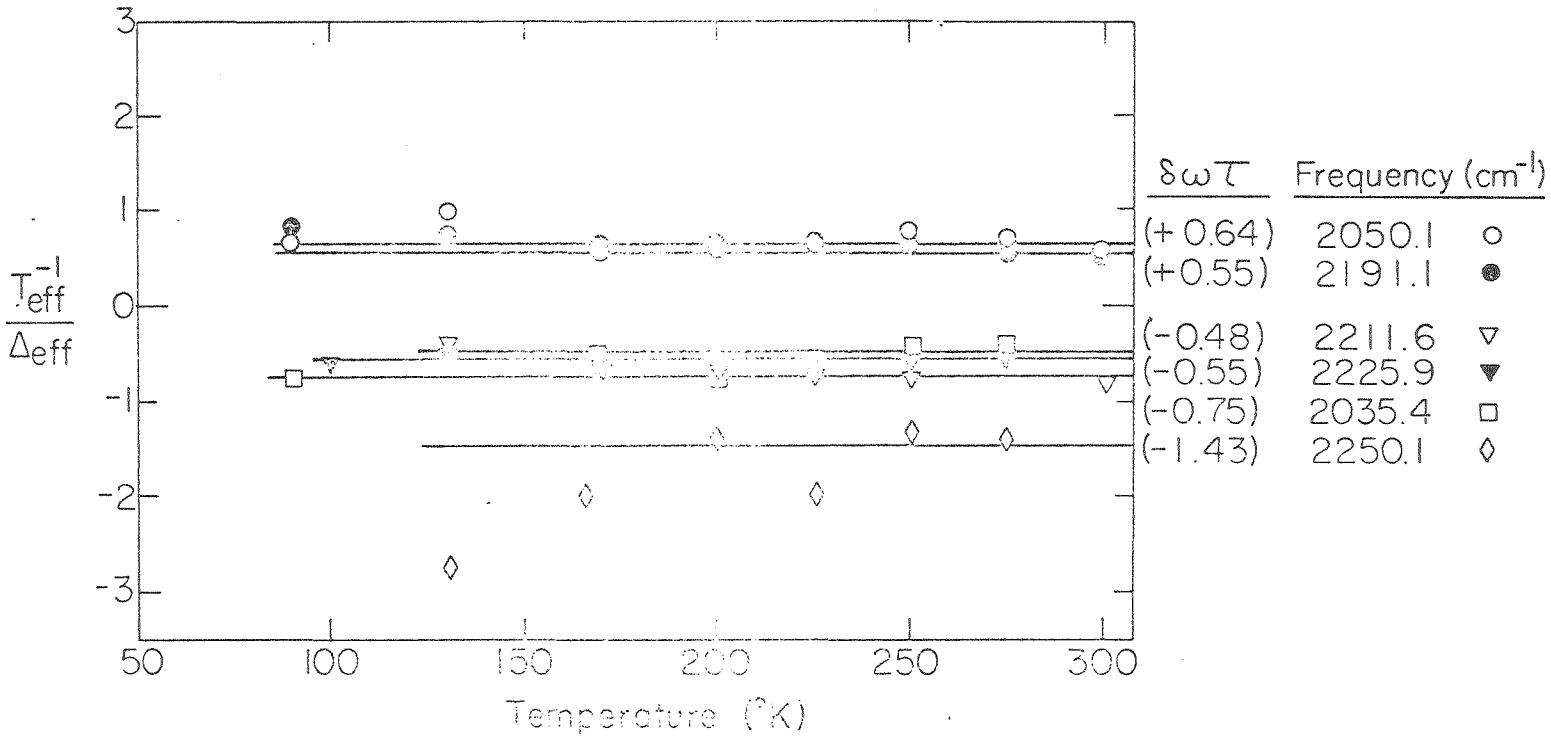

XBL 7911-7281

Figure 6

FREQUENCY SHIFTS OF TWO ISOLATED BANDS IN d_{14} - DURENE

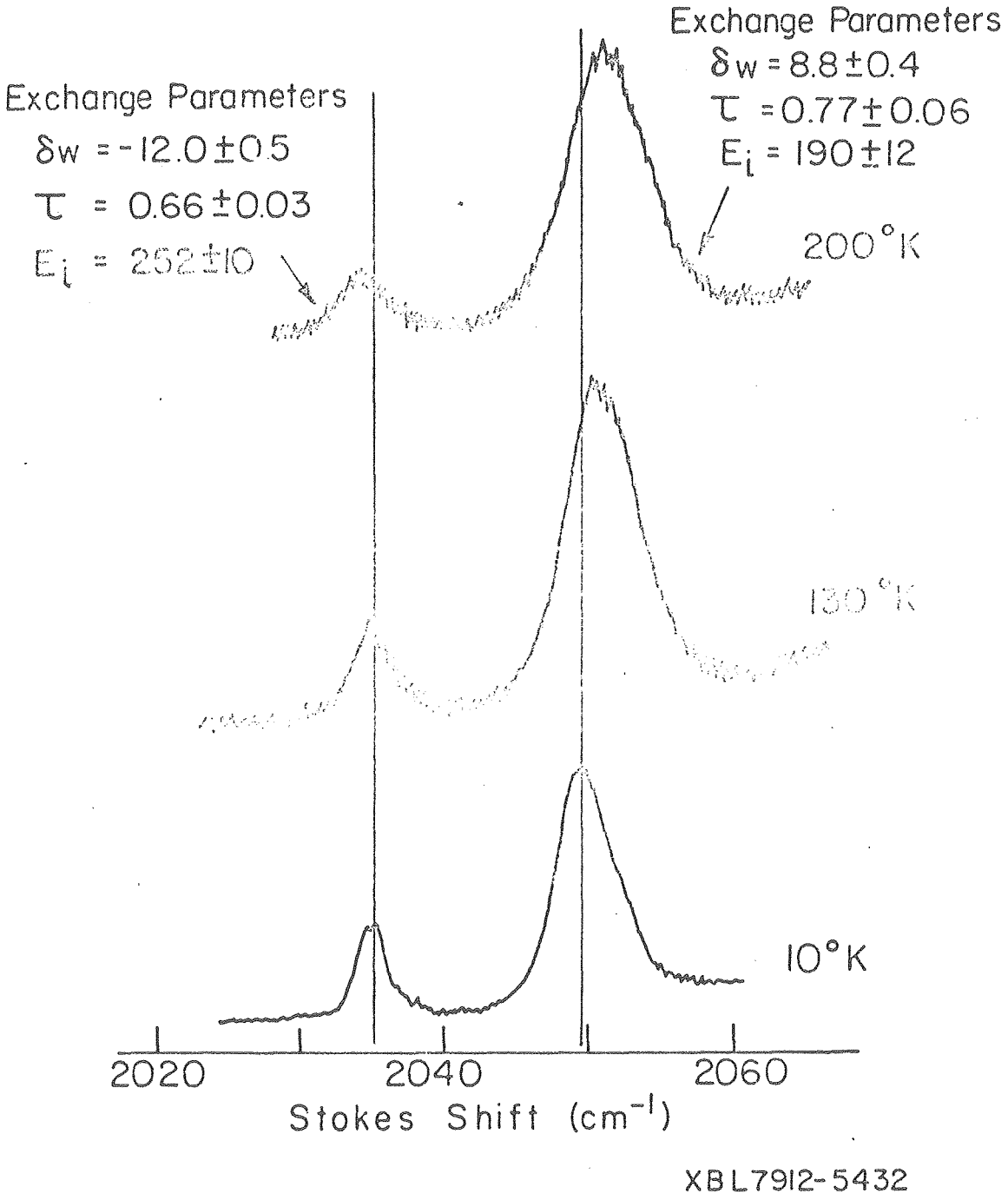

Figure 7

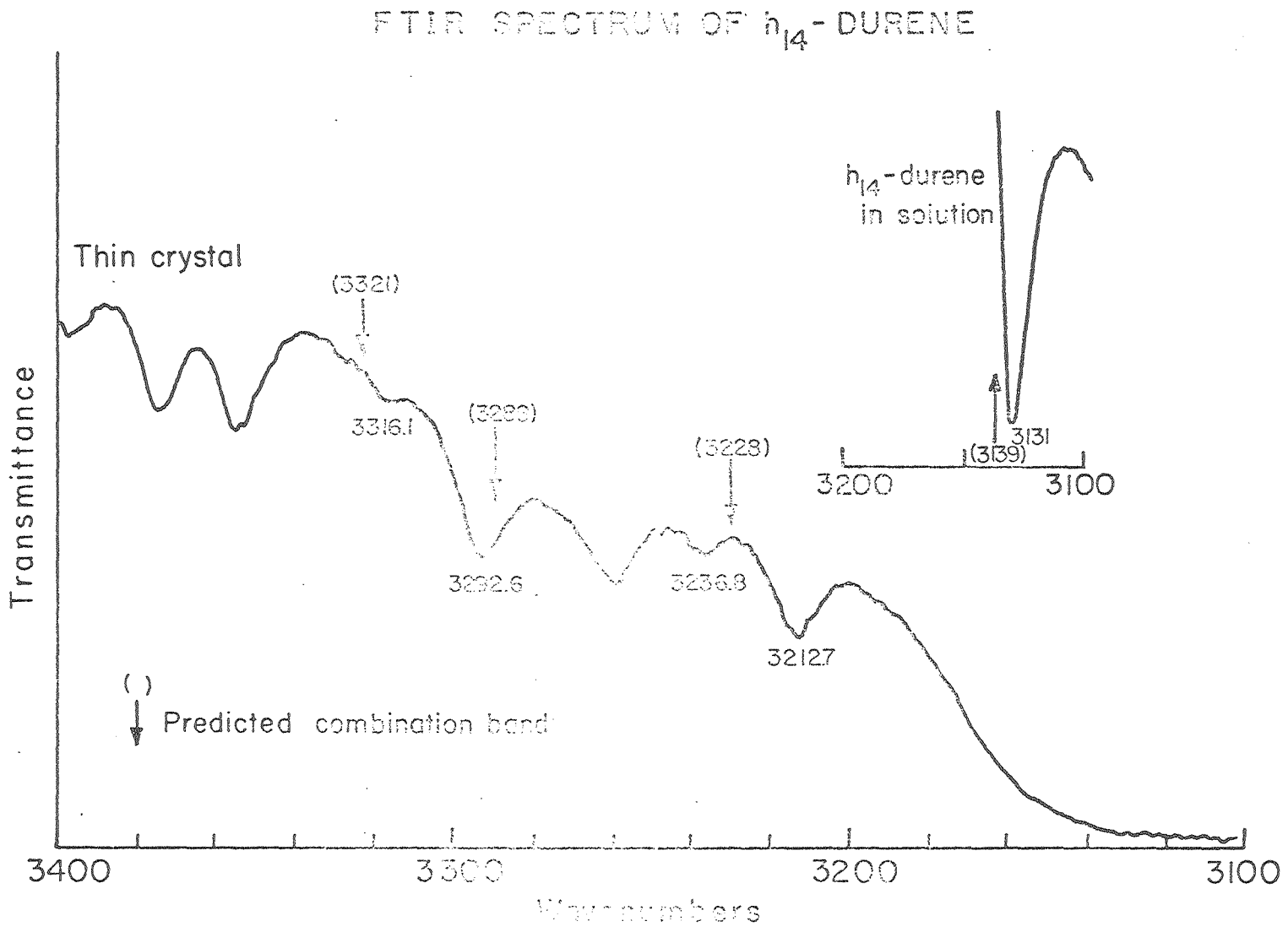
FTIR SPECTRUM OF h_{14}-DURENE
h_{14}-durene in solution
Thin crystal
(3321)
3316.1
(3280)
3282.6
(3228)
3236.8
3212.7
3131
(3139)
3200
3100
( )
Predicted combination band
Transmittance
3400
3300
3200
3100
Wavenumbers
XBL 7912-14591

Figure 3

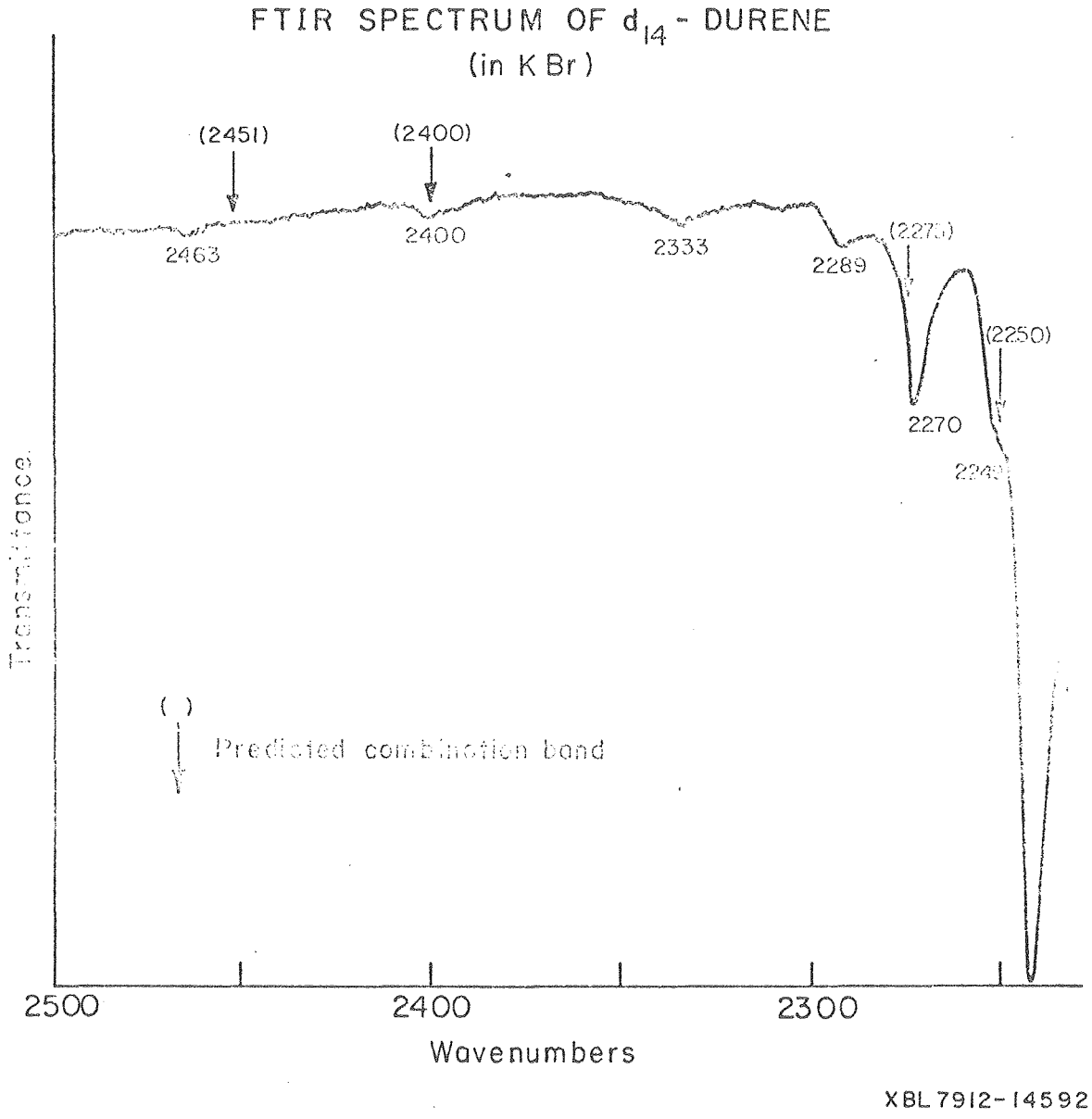
FTIR SPECTRUM OF d_{14} - DURENE
(in K Br)
(2451)
(2400)
2463
2400
2333
2289
(2275)
(2250)
2270
Transmittance
( )
Predicted combination band
2500
2400
2300
Wavenumbers
XBL 7912-14592

Figure 9

INTERMOLECULAR VIBRATIONAL DEPHASING IN DURENE

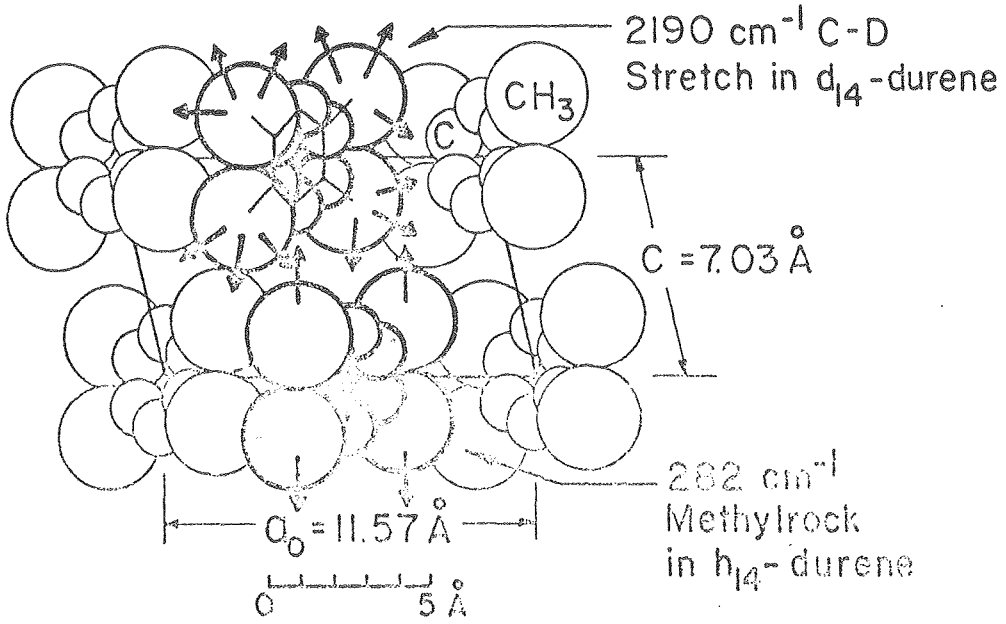

2190 cm^{-1} C-D Stretch of D_{14}-Durene
[Methyl D's]

Environment	$\Delta\nu$ (cm^{-1})	E_1 (cm^{-1})	T_1 (psec)
100% d_{14}-durene	19.5 ± 1	240 ± 10	0.30 ± .05
50% d_{14}-durene 50% h_{14}-durene	21.1 ± .5	260 ± 10	0.24 ± .03
25% d_{14}-durene 75% h_{14}-durene	22.4 ± .5	280 ± 10	0.21 ± .03
10% d_{14}-durene 90% h_{14}-durene	21.6 ± .3	285 ± 10	0.19 ± .03

XBL 7811-6183

Figure 10

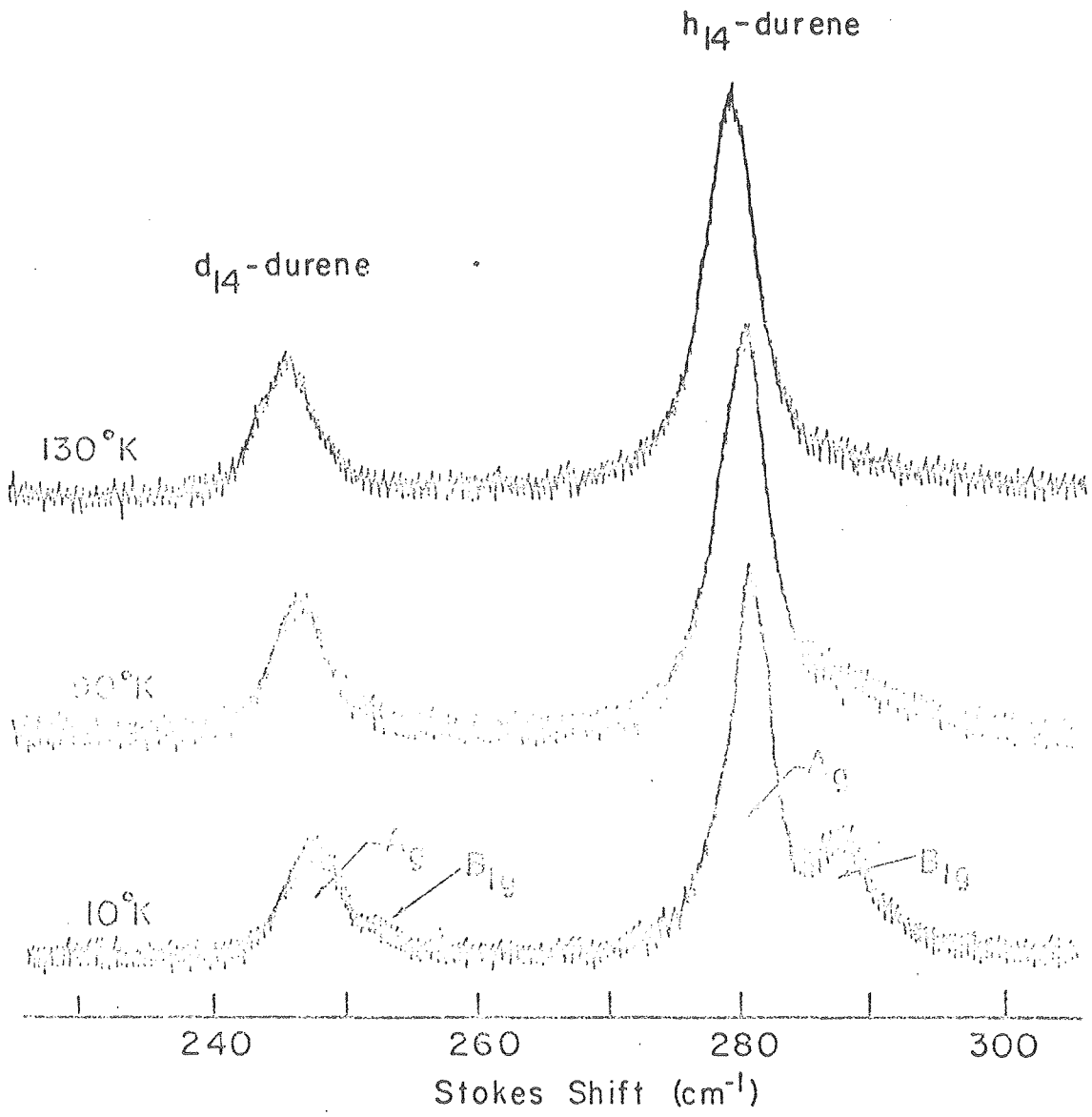
METHYL ROCK SPECTRA
IN 1:3 d_{14}: h_{14} - DURENE
h_{14}-durene
d_{14}-durene
130°K
50°K
10°K
B_{1g}
B_{1g}
240
260
280
300
Stokes Shift (cm^{-1})
XBL 794-6108

Figure 11

RAMAN ACTIVE IN-PLANE METHYL ROCKING MODES IN DURENE

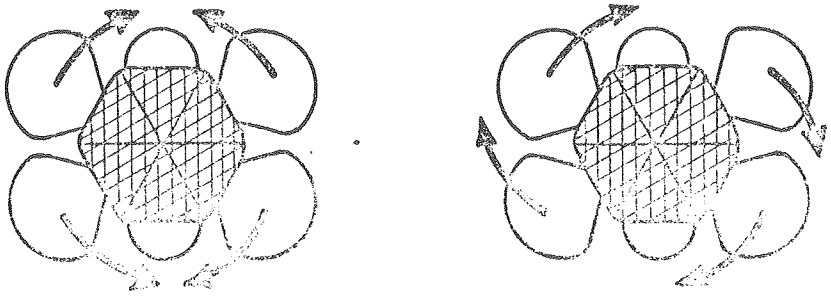

A_g Symmetry $\qquad$ B_{1g} Symmetry

Methyl Rock as Observed Dephasing Channel

	Peak $\tilde{\nu}$ (cm^{-1})	FWHM (cm^{-1})	T_2 (psec)	Symmetry of Methyl Rock
Pure h_{14}-durene	2970.5	263±6	0.13	A_g
	3027.5	265±15	0.36	B_{1g}
Pure d_{14}-durene	2035.4	252±10	0.66	B_{1g}
	2191.1	240±20	0.30	A_g
	2225.9	240±15	0.36	A_g

XBL794-6105

Figure 12

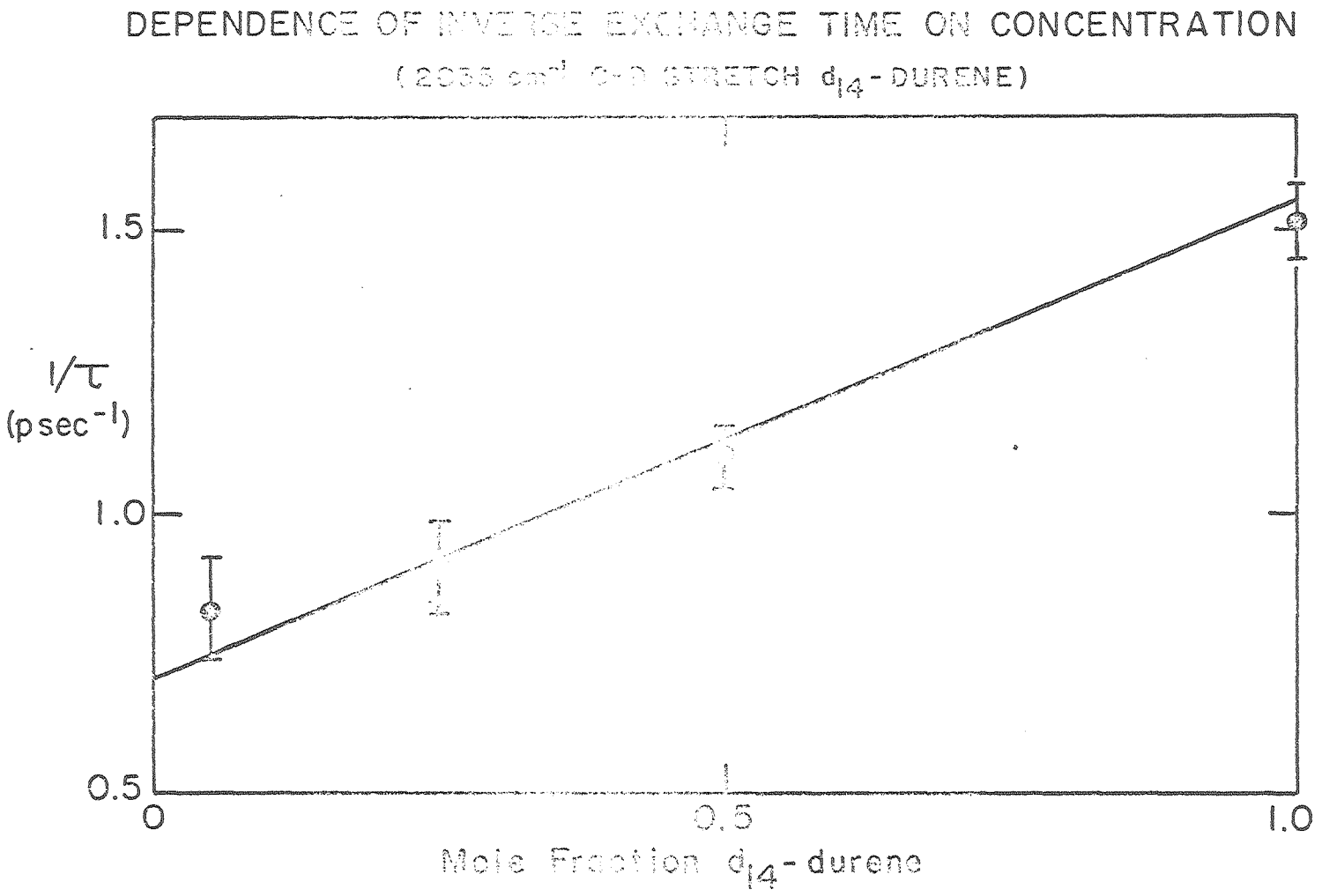
DEPENDENCE OF INVERSE EXCHANGE TIME ON CONCENTRATION
(2035 cm⁻¹ C-D STRETCH d14-DURENE)
1.5
1.0
0.5
1/τ
(psec⁻¹)
0
0.5
1.0
Mole Fraction d14-durene
XBL794-6106

Figure 13